Structure and dynamics of reverse micelles containing supercooled water investigated by neutron scattering

Tinka Spehr,[1,2,*] Bernhard Frick,[1] Isabelle Grillo,[1] Peter Falus,[1] Martin Müller,[2] and Bernd Stühn[2]
[1]*Institut Laue Langevin, BP 156, 38042 Grenoble Cedex 9, France*
[2]*TU Darmstadt, Hochschulstraße 8, 64289 Darmstadt, Germany*
(Received 6 October 2008; published 19 March 2009)

We present a detailed neutron scattering study of the structure, shape fluctuations, and translational diffusion of microemulsion droplets at low temperatures. We investigate the ternary microemulsion D_2O, AOT [bis(2-ethyl-hexyl) sulfosuccinate], and toluene-d8 (or heptane-d16) which forms spherical water droplets surrounded by a monolayer of AOT dispersed in oil around room temperature. At $T=290$ K, varying the molar ratio ω of water to AOT between 3 and 12, we find using small angle neutron scattering water core radii R_c between 7 and 18 Å, respectively. We characterize the structure at low temperatures down to $T=220$ K. Upon cooling the droplet structure is maintained and R_c stays roughly constant down to temperatures where the confined water is deeply supercooled. At an ω-dependent temperature T_s we observe for all compositions a shrinking of the droplets, which depends on the initial droplet size: the smaller the initial radii, the lower the T_s is. At the lowest investigated temperature $T=220$ K we find an ω-independent remaining water core corresponding to a number of about 2 water molecules per AOT molecule. Neutron spin-echo spectroscopy is used to monitor shape fluctuations and translational diffusion for one microemulsion ($\omega=8$, $R_w=12$ Å) from $T=300$ K down to temperatures below the corresponding shrinking temperature T_s. Thereby we determine the bending elasticity to be $\kappa=0.3k_BT$ over the whole investigated temperature range where the droplets are stable. From these results we cannot establish a link between surfactant membrane elasticity and low temperature structural instability of the droplets. Moreover, our results show that reverse AOT micelles are an excellent tool for the study of soft confined water over a broad range of confining sizes and temperatures down to the supercooled state.

DOI: 10.1103/PhysRevE.79.031404 PACS number(s): 82.70.−y, 47.57.jb, 61.05.fg, 68.05.Gh

I. INTRODUCTION

Microemulsions are homogeneous and thermodynamically stable mixtures of water and oil mediated by amphiphilic molecules called surfactants. The ternary system consisting of the anionic surfactant AOT [bis(2-ethyl-hexyl) sulfosuccinate], water, and oil is one of the most studied microemulsions [1]. Around room temperature for a large range of compositions it forms small spherical water droplets surrounded by a monolayer of AOT that are dispersed in the continuous oil matrix (see Fig. 1 for a sketch of such a reverse water swollen micelle). These reverse micelles are relatively monodisperse (polydispersity of 10%–20%) and by adjusting the molar ratio ω of water to surfactant one can change the micelle radius continuously in a controlled way between a few angstroms and several nanometers [2]. The density of droplets in the oil and hence the distance between droplets can be varied independently of ω by adjusting the droplet volume fraction ϕ. These droplet microemulsions therefore form good model systems for the investigation of liquids in soft confinement [3–5]. Due to its biological relevance a case of special interest is that of confined water [6] as many biological macromolecules enclose water and this nanoscale confined water is known to be essential for the stability and functionality of those molecules [7,8]. At the same time many studies using a broad range of different experimental techniques reveal that confined water differs substantially from bulk water concerning many physical properties [9]. A better understanding of biological systems containing water thus requires a deeper insight into the behavior of water under soft confinement. Besides giving access to spatial dimensions for which confinement effects can be expected it is also important that the confining environment remains stable over a wide temperature range and especially water in the supercooled state attracts interest for both fundamental and application reasons. But whereas the phase behavior and structure of this microemulsion is very well investigated around room temperature and for high temperatures, very little is known for temperatures below the freezing point of bulk water. Nevertheless without having a detailed knowledge about the structure and the dynamical behavior, water-in-oil microemulsions have been used for cryoenzymologic studies in the subzero temperature range

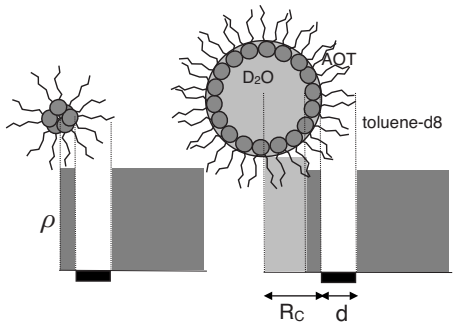

FIG. 1. Schematic coherent scattering length density ρ profile of an AOT reverse micelle and a D_2O swollen AOT reverse micelle in toluene-d8. Core radius R_c and shell thickness d are marked below the drawing.

*spehr@ill.fr

TABLE I. Literature data for freezing temperatures T_f^c of reverse micelle confined water obtained by different experimental techniques. ω denotes the molar ratio of water to AOT.

Solvent	Technique	ω	T_f^c	Ref.
Isooctane	DSC	1–10	$\omega \leq 4$: no freezing	[13]
Dodecane	DSC	1–20	$\omega \leq 6$: no freezing	[13]
			$\omega \geq 6$: freezing ~232 K	
			$\omega \geq 12$: continuous freezing from 253 K on	
TMB	DSC	3–38	2–4 H_2O/AOT remain unfrozen	[19]
Heptane	Fluorescent probing	0–30	Water core: ω dependent	[16]
			Shell water: ω independent, ~240 K	
Pentane	Infrared spectroscopy	1–40	ω independent, ~240 K	[17]

for more than 20 years now [10,11]. The first low temperature study on H_2O/AOT/iso-octane microemulsion with ω ranging between 0 and 60 was made using dynamic light scattering (DLS) [12]. The droplet size was determined in an indirect way by assuming that the spherical shape of the droplets is maintained at temperatures down to $T=178$ K and then the radius was calculated from the measured diffusion coefficient via the Stokes-Einstein relation. For samples with the lowest water content no change in size was observed for the whole investigated temperature range. Bigger water swollen micelles showed a size variation at a temperature already above $T=273$ K. Contradictory results were reported concerning the freezing of water in reverse AOT micelles for a variety of surrounding oils and molar ratios ω applying differential scanning calorimetry (DSC) [13–15], fluorescence probing [16], infrared spectroscopy [17], and neutron backscattering (3) [18]. A freezing temperature of the water core independent of the droplet size was reported [17] as well as a strong dependency of the supercooling on the confining size [18,16]. The results published on the freezing temperature of reverse micelle confined water are summarized in Table I. Furthermore the dynamics of the confined water was investigated for the D_2O/AOT/dodecane system with ω ranging from 3 to 38 from room temperature down to 230 K [19]. The reorientation rate of the supercooled confined water was found to be 2 orders of magnitude lower than that of bulk water at the same temperature. Results obtained by these different experimental techniques agree in the finding of a small amount of unfreezable water corresponding to two to six water molecules per AOT molecule and have in common that they only assume the preservation of the reversed micellar structure at all temperatures.

In this paper we present a detailed analysis of the structural and dynamical behavior of such microemulsion systems at low temperatures. We measured AOT-water microemulsion systems with different droplet sizes and toluene or heptane as oil down to $T=220$ K. By means of small angle neutron scattering we determined the size and polydispersity of the droplets as a function of temperature. We find the droplets to be stable down to temperatures much below the freezing point of bulk water. At a temperature T_s that depends on the initial water loading, and hence the size of the droplets, the droplets begin to shrink. The microemulsion structure has been investigated at such low temperatures in a direct way. This droplet instability temperature T_s is compared to results on water freezing. Even at the lowest investigated temperature $T=220$ K we observed a finite remaining water core whose size seems to be similar for all compositions and independent of the initial droplet water content. We discuss in detail the behavior of droplet polydispersity p, water core radius R_c, and AOT shell thickness d upon cooling. For two samples we also monitored the structure upon heating back to room temperature. We show that the structural changes observed upon cooling are reversible and that a continuous water uptake takes place beginning even at the lowest temperatures. To gain further insight into the mechanism of droplet shrinking we have chosen one microemulsion sample with an initial core radius of $R_c=12$ Å for performing neutron spin-echo (NSE) spectroscopy which is known to be an excellent tool for the determination of the bending elasticity of surfactant layers in microemulsion systems [20,21]. We discuss the translational diffusion coefficient of the entire droplets as well as the shell deformations and the deduced bending elasticity of the AOT surfactant membrane. We draw a consistent picture of the microemulsion structure and dynamics over the investigated temperature range. Our results will lay the groundwork for the study of water in confinement under well characterized conditions.

II. EXPERIMENTAL

A. Samples and materials

The microemulsions were prepared by mixing appropriate amounts of AOT, D_2O, and deuterated oil (toluene-d8, heptane-d16, or decane-d22) and shaking for several minutes until the samples were single phase and optically clear. Deuterated solvents n-heptane-d16, toluene-d8, n-decane-d22 (Acros Organics, Euriso-Top, 98%), D_2O (Euriso-Top, 99.9%), and AOT (Acros Organics) were used without further purification. The composition of the microemulsion is given by the two parameters ω and ϕ, with ω being the molar ratio of water to surfactant AOT and ϕ being the droplet (water plus AOT) volume fraction. The droplet radius depends on first approximation linearly on ω and is for moderate droplet concentrations independent of ϕ. In this study ϕ was kept constant at 0.2 (0.1 for NSE) while varying ω between 0 and 12 (8 for NSE). This ϕ was chosen to allow a

TABLE II. Summary of sample compositions of our study: ω denotes the molar ration of water to AOT; ϕ is the prepared droplet volume fraction.

Method	Sample	Composition	ω	ϕ
SANS	1	D_2O/AOT/n-heptane-d16	12	0.2
	2	D_2O/AOT/n-heptane-d16	5	0.2
	3	D_2O/AOT/n-toluene-d8	8	0.2
	4	D_2O/AOT/n-toluene-d8	3	0.2
	5	AOT/n-toluene-d8	0	0.2
	6	AOT/n-decane-d22	0	0.2
NSE	7	D_2O/AOT/n-toluene-d8	8	0.1

direct comparison with a neutron backscattering study on the freezing of water in reverse micelles [18]. In Table II compositions of all investigated samples are listed.

B. Small-angle neutron scattering

1. Technical

Small-angle neutron scattering (SANS) experiments were carried out on the D22 diffractometer at the Institut Laue Langevin (ILL, Grenoble, France) using a neutron wavelength of $\lambda=6$ Å. The ^{3}He multidetector (~ 1 m^2 active area with pixel size of 8×8 mm^2) was placed at a distance of 2 m from the sample (collimation of 8 m). The chosen configuration covered a range of scattering vectors $Q=4\pi/\lambda \sin(\theta/2)$ (with θ being the scattering angle) from 0.025 to 0.47 Å^{-1}. Samples were measured in 1 mm thick flat aluminum holders sealed with indium. A standard ILL orange cryostat was used for temperature control. For normalization to absolute intensities $I(Q)$ (cm^{-1}) the incoherent scattering of water in a 1 mm quartz cell was measured. The raw data were radially averaged, corrected for electronic background and empty cell scattering, and normalized to absolute intensities using standard ILL software [22]. Samples were cooled from $T=285$ down to 220 K with cooling rates of 0.5 K/min. While cooling scans were taken continuously with an accumulation time of 2 min/spectrum. In the investigated temperature range all used solvents are liquid (see Table II for a listing of bulk freezing points of the used oils).

2. Data analysis

For interacting polydisperse droplets of number density n with uncorrelated size and position the normalized SANS intensity (scattering cross section per unit volume) $I(Q)$ (cm^{-1}) can be written as the product of the average droplet form factor $F(Q)$ and a structure factor $S(Q)$ accounting for droplet-droplet interactions,

$$I(Q) = n\langle F(Q)\rangle S(Q) + I_{\text{inc}}, \tag{1}$$

where I_{inc} is the incoherent Q-independent background that was treated as a separate fitting parameter. The coherent scattering length densities ρ of the sample compounds were calculated as

TABLE III. Coherent scattering length densities ρ and bulk freezing temperature T_f for microemulsion compounds.

Compound	ρ (10^{-6} Å^{-2})	T_f (K)
D_2O	6.38	276.8
AOT_{head}	5.67	
AOT_{tail}	−0.38	
Toluene-d8	5.76	179
Heptane-d16	6.30	182
Decane-d22	6.64	241

$$\rho = \frac{1}{V}\sum_i b^i_{\text{coh}}, \tag{2}$$

where V denotes the molecular volume and b^i_{coh} denotes the coherent scattering length of atom i in the molecule [23]. Resulting values for ρ are listed in Table III. Since D_2O, the deuterated oil, and the AOT head groups have very similar coherent scattering length densities, the main contrast arises from the AOT tails. See Fig. 1 for a sketch of the scattering length density profile of a shell contrast water swollen reverse micelle and a pure AOT reverse micelle. We used a form factor $F(Q)$ for a polydisperse core-shell spherical particle with core radius R_c and shell thickness d [24], where the core is composed of D_2O and the AOT-head groups and the shell consists of the AOT tails (as visualized in Fig. 1),

$$F(Q) = \left[4\pi(\rho_c-\rho_s)R_c^3\left(\frac{j_1(QR_c)}{QR_c}\right)\right. \tag{3}$$

$$\left. + \; 4\pi(\rho_s-\rho_m)(R_c + d)^3\left(\frac{j_1[Q(R_c+d)]}{Q(R_c+d)}\right)\right]^2, \tag{4}$$

where j_1 denotes the spherical Bessel function of first order. Suffixes c, s, and m stand for core, shell, and matrix, respectively. For the fitting procedure ρ_c of D_2O and ρ_m of the deuterated oil were fixed to the theoretical values. The coherent scattering length density ρ_s of the AOT tails (shell) was allowed to vary between the calculated value and ρ_m as the oil is known to penetrate between the AOT tails. The droplet size polydispersity p,

$$p = \frac{\sqrt{\langle R_c^2\rangle - \langle R_c\rangle^2}}{\langle R_c\rangle}, \tag{5}$$

is accounted for by using in Eq. (1) a form factor $\langle F(Q)\rangle$ averaged over Schultz-Zimm distributed radii [25]. The factorization of $F(Q)$ and $S(Q)$ [Eq. (1)] strictly holds only for a system of monodisperse scatterers [26]. The effect on polydispersity on $S(Q)$ is, in Eq. (1), neglected. We used a structure factor $S(Q)$ for a hard sphere fluid with a narrow attractive well. In this model a perturbation parameter ϵ is defined as the ratio of the width of the attractive well to the total particle radius (hard sphere radius plus attractive well)

[27,28]. We have fixed ϵ to 0.05 and only the stickiness parameter τ was varied by the fitting procedure. The model curves are convoluted with the known instrumental resolution; this affects mainly the determination of the polydispersity [29]. Scattering curves were analyzed using the NIST package for analysis of SANS and USANS (ultrasmall-angle neutron scattering) data [30]. We want to underline that we fit the absolute normalized intensity. In Eq. (1) the droplet number density n is calculated with the droplet volume fraction ϕ and droplet volume $V_d=4/3\pi(R_c+d)^3$ as

$$n = \phi/V_d. \tag{6}$$

In principle ϕ is a known parameter defined by the sample composition. We nevertheless had to treat it as free fitting parameter, as ϕ depends sensitively on the absolute normalization of the intensity which is known to be only possible within an error of about 10% for SANS. Moreover the transmissions, needed for the normalization, have only been measured around room temperature. Fitting results for ϕ around room temperature were reasonably close (within 10%–20%) to the real prepared $\phi=0.2$.

C. Neutron spin echo

Technical

Neutron spin echo (NSE) directly measures the normalized intermediate scattering function $S(Q,t)/S(Q)$ (after resolution correction) with the Fourier time t,

$$t = \frac{\gamma Hlm^2}{2\pi h^2}\lambda^3 \tag{7}$$

with λ being the neutron wavelength, Hl being the magnetic field integral, h being the Planck constant, γ denotes the neutron gyromagnetic ratio, and m being the neutron mass (see elsewhere for a detailed explanation [31,32]).

The NSE experiments have been carried out at the spin-echo spectrometer IN15 at the ILL. The following configurations were used: a neutron wavelength $\lambda=6.3$ Å (10 Å) and scattering angles $2\theta=4.7°$, 7.7°, 10.7°, and 13.7° (4.7° and 7.7°) with a resulting Q ranging from 0.065 to 0.314 Å^{-1} (0.039–0.094 Å^{-1}), respectively. The resulting time window was 0–12 ns (50 ns). NSE decouples resolution and intensity to the first order; therefore a relatively large wavelength band of 15% [full width at half maximum (FWHM)] can be used. Samples were measured in the same flat aluminum sample holders of 1 mm thickness used for the SANS measurements. The temperature was controlled by a standard ILL orange cryostat and at all measured temperatures the sample was equilibrated for at least 1 h. The instrumental resolution was obtained by measuring graphite which is a coherent elastic scatterer. Resolution corrections were then simply carried out by dividing all sample spectra with the appropriate resolution measurement. All spectra were corrected for background scattering from the pure solvent and the sample holder. The detector is a 32×32 pixel ^{3}He multidetector located at a distance of 4.6 m from the sample. The multidetector signal was subgrouped into two to nine Q values per scattering angle 2θ.

TABLE IV. Summary of the temperature averaged fitting results for 20 vol % AOT reverse micelles dispersed in toluene-d8 (sample 5) and decane-d22 (sample 6). R_c denotes the core radius (AOT head), d is the shell thickness (AOT tail), ρ_s is the coherent scattering length density of the shell, and p is the polydispersity.

Sample	R_c (Å)	d (Å)	ρ_s (10^{-6} Å^{-2})	p (%)
5	2.1 ± 0.1	13.1 ± 0.1	1.1 ± 0.2	8.8 ± 0.2
6	2.7 ± 0.1	13.3 ± 0.3	-0.1 ± 0.2	9.8 ± 0.1

III. MICELLE STRUCTURE

In the following we discuss SANS results for reverse water swollen micelles with a constant volume fraction $\phi=0.2$ and molar ratio $3\leq\omega\leq12$ from room temperature down to $T=220$ K. For comparison we also studied pure reverse AOT micelles in deuterated oil. All investigated sample compositions are listed in Table II. Fitting results for AOT reverse micelles and microemulsion are shown in Tables IV and V, respectively. We describe the observation of a droplet instability, compare this to earlier studies of the freezing of confined water [18], and discuss the cooling-heating hysteresis.

A. Results and discussion

1. Structural behavior upon cooling

Figure 2 shows three representative spectra of sample 3 at temperatures of $T=297$, 250, and 230 K. For clarity curves

TABLE V. Fit results for microemulsion samples. R_c denotes the core radius, d is the shell thickness (AOT tail), and p is the polydispersity. Errors of the parameters are estimated to be $\Delta R_c\approx\Delta d\leq0.4$ Å and $\Delta p\leq0.3\%$.

Sample	R_c (Å)	d (Å)	p (%)
	$T=(280\pm1)$ K		
1	19.2	11.0	17.1
2	9.7	11.7	13.1
3	11.9	12.4	16.3
4	6.8	12.5	12.2
	$T=(260\pm1)$ K		
1	19.3	11.7	17.4
2	9.7	12.1	13.3
3	12.0	12.6	16.8
4	6.9	12.8	12.1
	$T=(230\pm1)$ K		
1	6.4	13.0	10.2
2	7.7	12.4	13.1
3	5.4	11.1	10.1
4	6.4	12.5	13.4

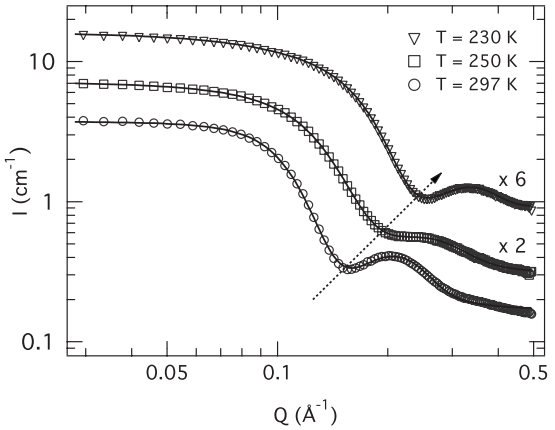

FIG. 2. Scattering from sample 3 (D_2O/AOT/toluene-d8, $\phi=0.2$, $\omega=8$) at three different temperatures. Solid lines are fits to the described form factor plus structure factor model. For clarity curves are shifted vertically by a factor shown close to the right axis. With decreasing temperature the micelles decrease in size (shown by arrow, see text for further explanations). Error bars are smaller than the symbols.

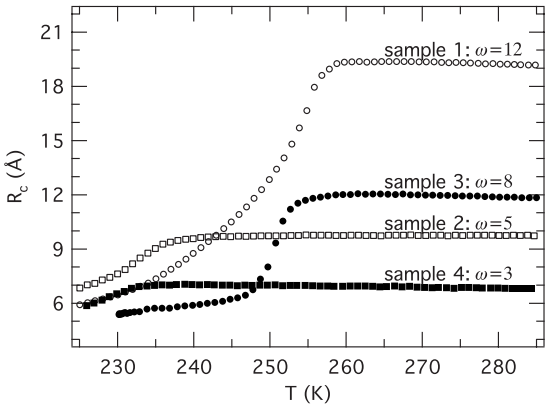

FIG. 3. Core radii of water swollen micelles as a function of temperature. Sample names as introduced in Table II are written above each curve. Error bars are smaller than the symbols.

are vertically shifted by factors indicated close to the right axis. Solid lines are fits to the model explained in Sec. II B 2. The above mentioned core-shell model describes all data very well over the whole investigated temperature range. The reverse micellar structure seems to be preserved, only the size of the droplet changes. With decreasing temperature the droplet size shrinks which is revealed by a clear shift of the form factor minimum to higher Q as emphasized by the arrow in Fig. 2. From the fitting we obtain the following parameters: the core radius R_c, the thickness d of the shell formed by the AOT tails, and the droplet size polydispersity p. As we work with a moderate droplet volume fraction $\phi=0.2$ we do not see a strong effect of droplet interactions which would reveal itself by a structure factor peak at low scattering vector Q. Nevertheless the inclusion of a sticky hard sphere structure factor led to a significant increase in the fit quality at low Q as our model describes the scattering intensity in absolute units. A slight increase or decrease in the absolute intensity essentially at smaller Q is caused by droplet interactions. We found that the inclusion of the structure factor did not have a significant effect on the form factor parameters. Due to the rather flat structure factor we think that no unambiguous conclusions can be drawn from the fitting parameters of the structure factor without further experiments under variation in ϕ. We therefore do not further discuss the structure factor parameters (stickiness τ and perturbation parameter ϵ) in this context. Our main interest is the confinement size as defined by the droplet core radius R_c with changing temperature. In Fig. 3 R_c of all investigated samples is plotted as a function of temperature. It can be seen that the initial R_c remains unchanged with decreasing temperature even below the freezing point of bulk deuterated water. At a well defined temperature T_s the radii R_c abruptly start to decrease and then tend to a plateau value at low temperatures. We determined T_s as the temperature where the droplet core radius R_c drops 0.3 Å below the high temperature average radius. Whereas the temperature T_s and the kinetics of shrinking (slope of the curve) depend on the sample composition, R_c seems to converge to the same low temperature R_c for all compositions. For all samples investigated we observe a remaining finite core radius of about $R_c \approx 5-6$ Å. The temperature T_s is found to be a function of the molar ratio ω. The smaller the ω is and hence the smaller the initial droplets are, the lower the temperature T_s is down to which the droplet size remains stable. The shrinking of the droplets below T_s is probably caused by water expulsion as investigated in detail by [33].

2. Relation between droplet instability and freezing behavior of confined water

Recently we investigated the freezing behavior of water confined in reverse AOT micelles [18]. Elastic scans on neutron BS showed that the freezing point of the confined water is depressed. It was found that the supercooling depends on the size of the micelles: the smaller the micelles are, the lower the freezing temperature of the enclosed water is. An interesting question is now if and how the structural instability of the reverse micelles relates to the freezing behavior of the water confined in the micelles. We define the supercooling ΔT_{BS} as determined by BS to be:

$$\Delta T_{\mathrm{BS}} = T_f - T_f^c \tag{8}$$

with T_f and T_f^c being the freezing temperatures of bulk and confined water, respectively. This quantity is compared to ΔT_{SANS},

$$\Delta T_{\mathrm{SANS}} = T_f - T_s \tag{9}$$

being the difference between the freezing temperature T_f of deuterated water and the shrinking temperature T_s of the droplets as observed in Fig. 3. In Fig. 4 we plot ΔT from both experimental methods as a function of the droplet core radius R_c. Hollow symbols are BS results and full symbols are SANS results. It turns out that both data sets for ΔT follow the same functional dependency on the radius R_c. We again want to underline that Fig. 4 compares structural findings and thus a static characteristic of the system (ΔT_{SANS}) with a dynamic observable (ΔT_{BS}). In this context it has to

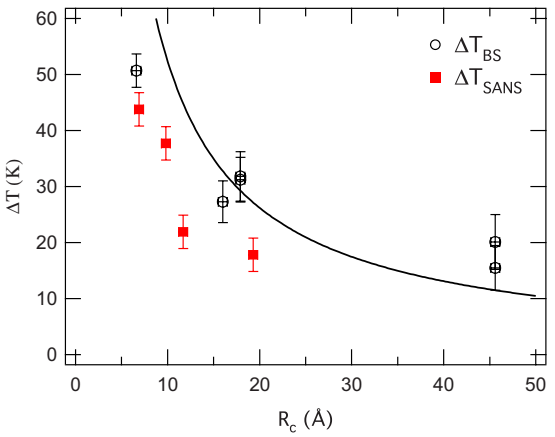

FIG. 4. (Color online) Supercooling ΔT as a function of micelle core radius R_c. Hollow symbols are results from elastic scans on backscattering [18]; full symbols correspond to SANS. Solid line shows the Gibbs-Thomson dependency [Eq. (10)] with the theoretical constant $K_{GT}=524$ K Å.

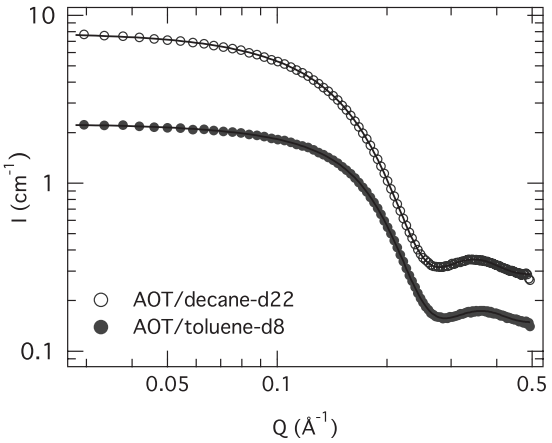

FIG. 5. Scattering from 20 vol % AOT reverse micelles dispersed in toluene-d8 (●, sample 5, $T=278$ K) and decane-d22 (○: sample 6, $T=283$ K, shifted by a factor 2). Error bars are smaller than the symbols. Solid lines are fits to a core-shell form factor combined with structure factor (see Sec. II B 2).

be mentioned that cooling rates for BS experiments were in the order of 0.3–0.5 K/min, thus very similar to those applied for the SANS experiments. The main experimental difference is the thickness of sample holders which was ten times thinner in the case of BS (0.1 mm). If we assume that the ice formation occurs inside the droplets by the mechanism of homogenous nucleation then we can relate the supercooling to the confining radius R_c. Freezing of the water should only be possible at the temperature where the critical radius of an ice nuclei gets smaller than the radius R_c of the water core. Note that the size of the critical nucleus depends on temperature. The supercooling ΔT can now be expressed as a function of the droplet radius R_c [34],

$$\Delta T \approx \frac{2\gamma_{sl}T_f}{\rho L_{sl}R_c} = \frac{K_{GT}}{R_c} \tag{10}$$

with L_{sl} and γ_{sl} being the heat of fusion and surface tension between liquid water and ice, respectively, and ρ being the density of water. Equation (10) is known as the Gibbs-Thomson equation and it predicts the supercooling ΔT to be inversely proportional to the radius R_c. Inserting the values for γ_{sl} and L_{sl} of water at its bulk freezing temperature T_f we estimate the constant $K_{GT}=524$ K Å [34] (and references therein). The solid line in Fig. 4 is a plot of the Gibbs-Thomson dependency without any adjustable parameter. The supercooling ΔT_{BS} for radii $R_c>10$ Å is reasonably well described by that relationship, although the use of K_{GT} can only be a rough estimation since it does not take into account the temperature dependence of the involved constants. Recently it was shown that the melting point depression of water confined in mesoporous silica follows Eq. (10) when taking into account a layer of nonfreezable water close to the walls [34]. Hard and soft confinements thus seem to have similar effects on water freezing. We will restrict ourselves to this qualitative discussion of ΔT_{BS} as the error bars and the number of our data points does not allow to deduce further information about a surface layer by fitting. For a detailed discussion of the effect of dissolved AOT Na^+ counterions on the water freezing we refer to our previous work [18]. There we showed that the observed supercooling of the water is not explainable by dissolved foreign particles.

3. Remaining water core radius at low temperatures

For comparison with the shrunken water filled reverse micelles we studied as well pure reverse AOT micelles. Samples with an AOT volume fraction $\phi=0.2$ in two different oils (toluene-d8 or n-decane-d22; see Table II) were investigated between $T=290$ and 260 K. Figure 5 shows two representative spectra at $T\approx 280$ K. The data were fitted with a core-shell model for the form factor combined with a sticky hard sphere structure factor as explained in Sec. II B 2. The scattering length density of the core, composed of AOT heads, and the solvent (toluene-d8 or n-decane-d22) were fixed to the theoretical values. The scattering length density ρ_s of the shell composed of the AOT chains was allowed to vary between the calculated value and ρ_m oil as the oil is expected to interpenetrate between the chains. Table IV lists the temperature averaged fit results and Fig. 6 displays their variation with temperature. For the head group we find a thickness of about 2.5 Å, which compares well with values found by others [5,35]. The thickness of the shell composed of the AOT chains seems to increase slightly with cooling starting at $d=13$ Å at $T=290$ K. This can be explained by the hydrocarbon chains becoming stiffer with decreasing temperature. The average distance between the chains is determined by competition between van der Waals attraction and steric (entropic nature) repulsion. The former is less sensitive to temperature, whereas the latter decreases upon cooling (chain fluctuations responsible for steric repulsion are weaker for more rigid chains). Upon cooling the average interchain distance thus becomes smaller and the shell becomes less penetrable. This is also reflected by the decreasing scattering length density ρ_s of the shell. The higher absolute value for the scattering length density ρ_s of the AOT chains in toluene is due to the better penetration of the chains by the smaller toluene molecule [36]. The size of

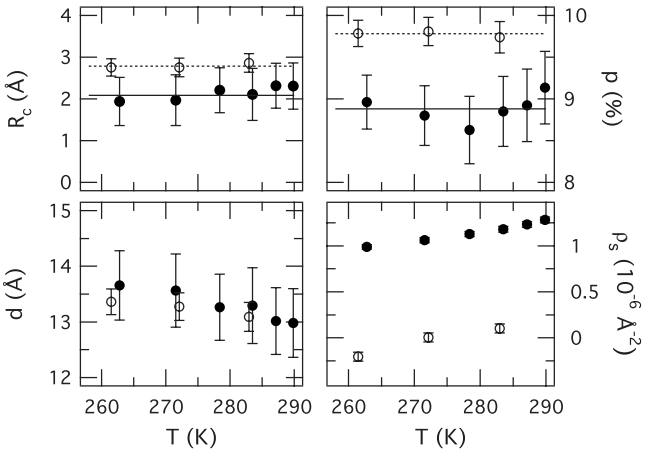

FIG. 6. Fitting parameters for AOT reverse micelles dispersed in toluene-d8 (●, sample 5) and decane-d22 (○: sample 6). Core radius R_c, polydispersity p, shell thickness d, and scattering length density ρ_s of the shell.

the micelles $(R_c+d)\approx 15$ Å (core and shell) lies close to the values published for the linear length of the AOT molecule of 12 Å. These findings compare well with results from DLS experiments on AOT micelles in iso-octane which showed a temperature independent micelle radius of 15 Å between $T=250$ and 370 K [12] and SANS measurements finding the length of AOT to be about 16 Å [37]. In both oils the micelles are very monodisperse: over the whole investigated temperature range we find a polydispersity in size of $p=9\%-10\%$. Very recently frozen solutions of AOT/n-heptane have been investigated by small angle x-ray scattering (SAXS) [38]. These authors conclude that while at $T=77$ K the reverse micelle structure is maintained and the micelles undergo a clustering process. The published value of around 10 Å for the radius of the core consisting of the head groups disagrees with our results. Our findings are consistent with the established dimensions of AOT.

Turning now to the water swollen reverse micelles we want to know if the shrunken micelles at low temperature still contain water. All investigated microemulsion compositions agree in showing a remaining core radius of more than 5 Å even at the lowest temperatures $T=220$ K. Due to the similar scattering length densities ρ of D_2O and AOT-head groups we cannot distinguish between them by means of SANS. The core radius determined for the water swollen micelles is thus composed of both. Only the direct comparison with the size of the AOT-head group as identified by measuring the pure AOT micelles under the same conditions allows us to draw conclusions on the amount of remaining water. By subtracting 2.7 Å, the maximum value determined for the size of the AOT-head group, we know that a minimum water core of more than 2.3 Å survives after the shrinking of the droplets. This value corresponds approximately to a number of 2 water molecules per AOT [35] and confirms the previously discussed observations of two to four unfreezable water molecules per AOT [19].

4. Reversibility upon heating

We tested the reversibility of the observed structural changes upon heating for samples 3 and 4. After 15 min of equilibrating at the lowest temperature the samples were heated back to $T=290$ K with a heating rate of 0.5 K/min. The data were analyzed as explained in Sec. II B 2. In Fig. 7 the obtained form factor fitting parameters for cooling and heating are compared for both samples. Full symbols represent cooling results and hollow symbols represent heating results as a function of temperature. Results for samples 3 and 4 are shown on top and bottom of the figure, respec-

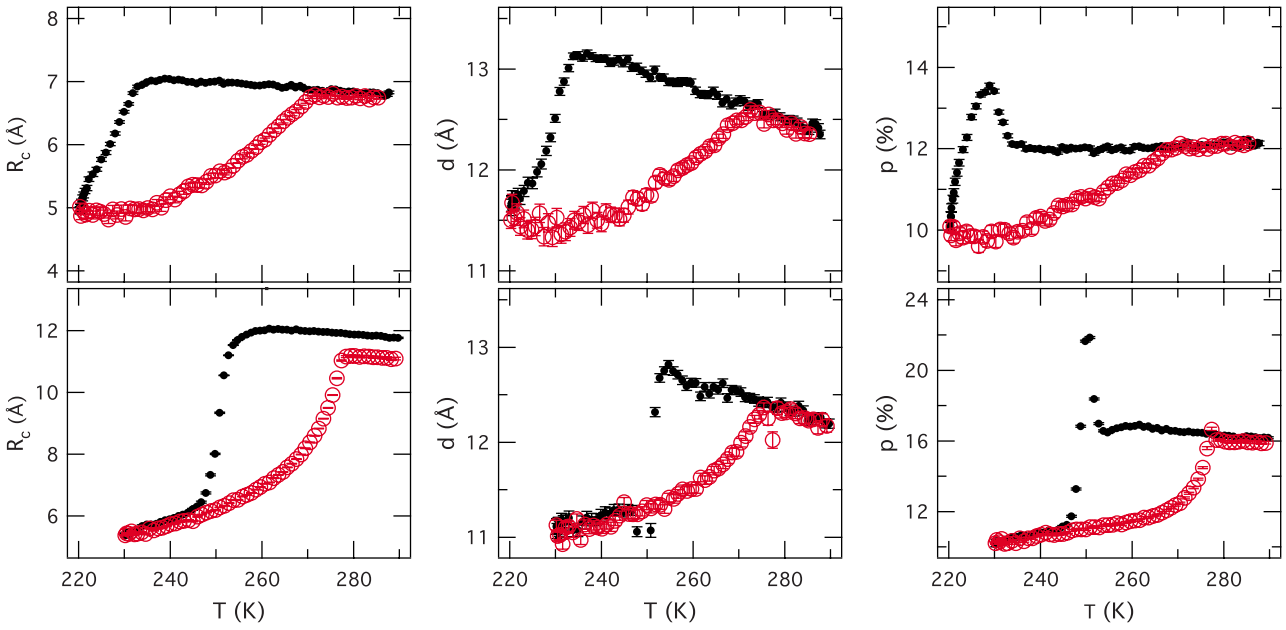

FIG. 7. (Color online) Sample 4 (figures in first line) and sample 3 (figures in second line): radius R_c, shell thickness d, and polydispersity p upon cooling (full symbols) and heating (hollow symbols). Cooling and heating rates: 0.5 K/min. Note the hysteresis: cooling and heating curves are in good agreement only above $T\approx 275$ K.

tively. For both samples we find that structures upon heating and cooling are different. They become similar only for temperatures above $T=270$ K only. Form factor fitting parameters that describe the structure show a pronounced hysteresis.

Core radius R_c. Discussing the parameters in the order they are shown in Fig. 7 we will start with the core radius. R_c falls back on its starting value after the cooling and heating cycles for sample 4; in the case of sample 3 the final radius lies about 1 Å below the initial value. Another important finding is that for both samples the droplets grow upon heating already from the lowest temperatures on. This means that far below the freezing point of bulk water the droplets rapidly incorporate the water that was ejected in the cooling scan. This is in contrast to observations by Simorellis *et al.* [33] who reported a much slower water uptake corresponding to $\omega=1/\text{day}$ when the samples are not agitated which was also the case in our experiment. However, these results cannot be compared directly to ours as a different oil was used and the sample holder geometry can probably have an impact on the kinetic behavior of the samples.

AOT shell thickness d. For both droplet sizes cooling leads first to a small increase in the shell thickness d. As discussed in Sec. III A 3 this reflects the increasing rigidity of the hydrocarbon tails with decreasing temperature. Exactly at the temperature where we observe the shrinking of the droplet radius R_c the shell thickness d abruptly decreases for both samples. This finding may suggest that the hydrophobic AOT tails collapse when water is expelled. Upon heating the AOT tails continuously stretch out again until they reach their initial size around $T\approx 275$ K. Some influence of a change in scattering length density cannot be excluded either. Above $T\approx 275$ K heating and cooling curves lie on top of each other.

Size polydispersity p. The last parameter shown is the polydispersity p of the radius R_c. In unison both samples show upon cooling a constant p down to roughly the respective shrinking temperature T_s. There we observe a sudden increase in the polydispersity p. This peak in p may be the signature of a system consisting of bigger and smaller droplets. Whereas R_c shows that the mean droplet radius R_c decreases from T_s on, the analysis of p reveals the coexistence of different sized droplets at the temperature range of transition from big to small droplets. Upon further cooling the polydispersity falls down to $p\approx 10\%$ at the lowest investigated temperature. This value is still slightly bigger than the previously discussed polydispersity $p\approx 9\%$ of pure AOT micelles dispersed in toluene-d8 shown in Fig. 6. Heating the samples up leads to a continuous increase in the polydispersity and again the values observed for p while cooling are reproduced above 275 K. Note that except for the slightly smaller final radius of sample 3 all other parameters fall back on the starting values after the cooling-heating cycle.

IV. MICELLE SHELL FLUCTUATIONS AND DIFFUSION

Up to now we only discussed the static (time-averaged) structure of the microemulsion as seen by the SANS snapshots. Over time microemulsion droplets continuously fluctuate around their mean shape and they diffuse in the surrounding oil. These thermal activated small fluctuations around a time-averaged mean spherical droplet form can be expressed by an expansion into spherical harmonics [21]. The dimensionless amplitudes and relaxation rates of the deformations can be derived (besides the diffusion constant of the whole droplet) from the time constants measured by NSE. From these parameters, together with structural information obtained by SANS, the bending elasticity κ of the AOT shell can be accessed. Typically values below $\kappa \leq 0.1k_BT$ are found to result in microemulsion instability. Therefore the above described droplet shrinking at low temperatures motivates us to search for a possible relation between the bending elasticity and droplet instability. Droplet microemulsions have extensively been studied by NSE [39–41] and especially water swollen AOT micelles with variety of different surrounding oils and molar ratios ω have been subject of a number of investigations [41–45]. Published values for κ in water/AOT/oil systems range from $0.2k_BT$ to several k_bT as summarized, e.g., in [42]. To our knowledge no such investigations were reported for low temperatures ($T<270$ K) and none for toluene as oil. For the investigation of the relationship between the bending elasticity κ of the AOT shell and the structural stability of the droplets one sample composition was chosen: AOT/D_2O/toluene-d8 with $\omega=8$ and $\phi=0.1$. The SANS experiments showed that for this composition the initial core radius $R_c=12$ Å is stable down to $T_s\approx 255$ K. For the NSE experiment we thus varied the temperature between $T=300$ and 250 K to cover the range where the shrinking of the droplets does occur.

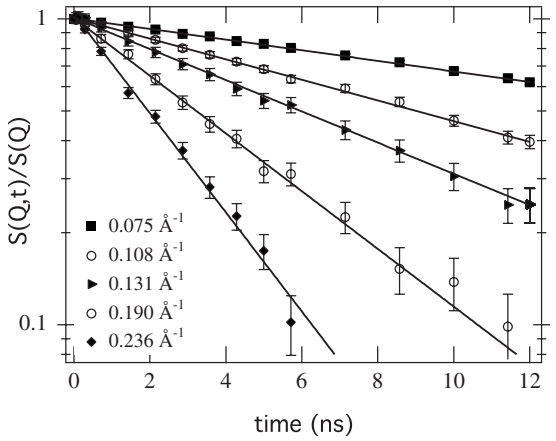

FIG. 8. Normalized intermediate scattering function $S(Q,t)/S(Q)$ at $T=265$ K. Scattering vectors Q are indicated next to symbols. Solid lines are fits to a single exponential function.

A. Results and discussion

In Fig. 8 normalized intermediate scattering functions $S(Q,t)/S(Q)$ for the microemulsion at a temperature of $T=265$ K are shown for a selection of scattering vectors Q. By fitting the intermediate scattering function to a single exponential we obtain an effective diffusion coefficient D_{eff},

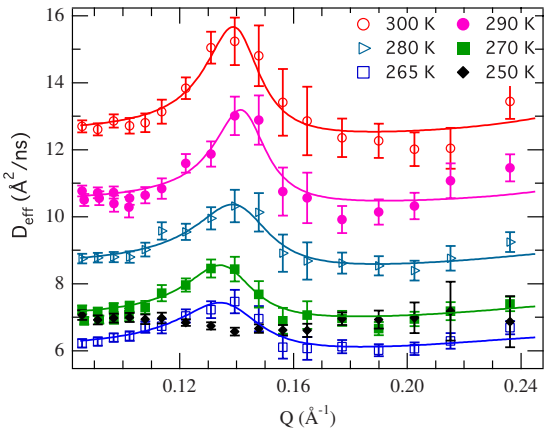

FIG. 9. (Color online) Effective diffusion coefficient D_{eff} as obtained by fitting the NSE curves to a single exponential [Eq. (11)]. Solid lines are fits to Eq. (12). Note that no maximum around $Q=0.14$ Å^{-1} is observed at the lowest temperature $T=250$ K.

$$\frac{S(Q,t)}{S(Q)} = \exp[-D_{\mathrm{eff}}(Q)Q^2 t], \tag{11}$$

where D_{eff} contains the Q-independent translational diffusion coefficient D_{tr} and a Q-dependent term $D_{\mathrm{def}}(Q)$ representing the droplet shape fluctuations [46],

$$D_{\mathrm{eff}}(Q) = D_{\mathrm{tr}} + D_{\mathrm{def}}(Q), \tag{12}$$

$$D_{\mathrm{def}} = \frac{1}{Q^2}\frac{5\lambda_2\langle|u_2|^2\rangle F(QR)}{\{4\pi[j_0(QR)]\}^2 - 5\langle|u_2|^2\rangle F(QR)} \tag{13}$$

with

$$F(QR) = [4j_2(QR) - QRj_3(QR)]^2. \tag{14}$$

Here the small droplet fluctuations around a time-averaged spherical shell are described by an expansion in spherical harmonics up to the mode $l=2$. j_l denotes the lth spherical Bessel function, λ_2 denotes the relaxation rate, and $\langle|u_2|^2\rangle$ denotes the mean squared amplitude of the $l=2$ mode. Solid lines in Fig. 8 are fits to a single exponential in order to extract the previously discussed effective diffusion coefficient D_{eff}. Note that the single exponential function describes our data in an adequate way. The thereby extracted effective diffusion coefficients D_{eff} for the microemulsion droplets are shown in Fig. 9 as a function of the scattering vector Q. From top to bottom the temperature varies from $T=300$ to 250 K. Indeed we observe a clear maximum of D_{eff} around $Q=0.14$ Å^{-1} for all temperatures except $T=250$ K. Let us here recall that for the studied composition the shrinking of the droplets was observed around 255 K. For all temperatures above 255 K the sample thus consists of droplets dispersed in toluene with a core radius $R_c=12$ Å whereas at 250 K the water core is diminished to 6–7 Å. Adding on that the thickness d of the AOT shell the total core radius (R_c+d) changes from 25 to 19 Å. The solid lines in Fig. 9 are fits to the Q dependence of D_{eff} as described by Eq. (12). The resulting parameters of the fit versus the temperature are displayed in Fig. 10. It should be mentioned that when using Eq. (12) for the description of the shell fluctuations we neglect the higher order deformations $l>2$. This can explain the small discrepancies between the model and D_{eff} for $Q>0.2$ Å-1.

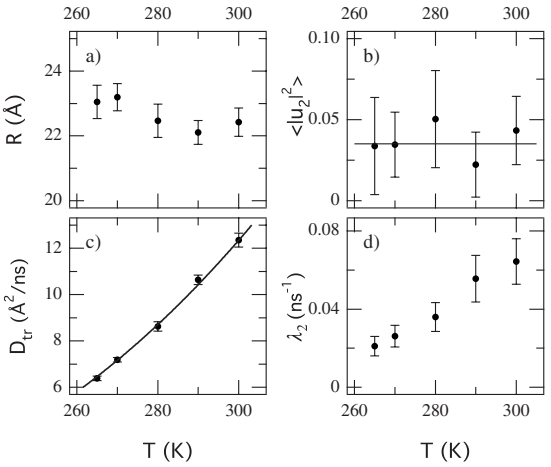

FIG. 10. Temperature dependencies of fitting parameters of Eq. (12). (a) Mean droplet radius R, (b) dimensionless fluctuation amplitude $\langle|u_2|^2\rangle$, (c) translational diffusion coefficient D_{tr}, the line is a fit to Eq. (15), and (d) relaxation rate λ_2 of second order oscillation.

Droplet radius. The location of the maximum Q_{max} of D_{eff} is determined by the mean radius R of the fluctuating shell. In Fig. 9 it can be seen already with the naked eye that this maximum slightly shifts between the different temperatures. Figure 10(a) displays the fitting results for R as a function of temperature. Below 280 K the radius seems to increase of about 1 Å from $R_c=22.2$ to 23.1 Å. Due to the relatively large errors we do not attach too much importance to these small changes, though we note that also the SANS experiments show that the thickness of the AOT shell (thus also the total radius) increases slightly with decreasing temperature. But contrary to the NSE results the SANS results show a continuous variation with temperature and much smaller relative errors. The absolute value for the NSE radius of about 22–23 Å is in good agreement with the 25 Å observed by SANS.

Diffusion coefficient D_{tr}. The level of D_{eff} at small Q gives the translational diffusion coefficient D_{tr} [Fig. 10(c)]. D_{tr} can be related by the modified Stokes-Einstein equation to a hydrodynamic radius R_h of the diffusing droplet [47],

$$D_{\mathrm{tr}} = (1-\phi)\frac{k_b T}{2\pi\eta_t R_h}\frac{\eta_w+\eta_t}{3\eta_w+2\eta_t}, \tag{15}$$

where ϕ denotes the volume fraction of droplets and η_t and η_w denote the temperature-dependent viscosities of toluene-d8 and heavy water, respectively. The viscosity η_t of deuterated toluene in the temperature range of interest was assumed to be similar to that of protonated toluene as given in [48]; η_w of heavy water was calculated from the viscosity of protonated water found in [49] with the formula given in [50]. From the SANS experiments we know that neither the geometrical radius nor the interactions of the droplets significantly change with temperature (above 255 K). The variation in D_{tr} with temperature should then be completely contained in the temperature dependence of the toluene and water vis-

cosities η_t and η_w and the only free parameter in Eq. (15) is R_h. In effect the absolute value of D_{tr} can for all temperatures above 255 K be expressed in an excellent way by the modified Stokes-Einstein equation and a constant temperature independent R_h of 33 Å, shown by the solid line in Fig. 10(c). The deduced R_h is about 1.3 times larger than the geometrical radius (R_c+d) of the droplets determined by SANS. A hydrodynamic radius R_h bigger than the geometrical radius has been observed in many different micelle systems and is explained by a shell of solvent molecules that moves along with the diffusing droplet [51]. Turning our attention now to the behavior of D_{eff} at 250 K shown in Fig. 9 we remark that the effective diffusion coefficient D_{eff} is rather Q independent and flat. At first glance it is surprising to see that despite the higher viscosity of toluene at $T=250$ K the D_{eff} is bigger than at 265 K. We estimate the translational diffusion coefficient D_{tr} at $T=250$ K by Eq. (15) taking into account the hydrodynamic radius of about 1.3 times the total geometrical radius $R_h \approx 1.3(R_c+d)=24$ Å and the droplet volume fraction that is due to the water expulsion reduced to $\phi \approx 0.08$. We get $D_{\mathrm{tr}}=6.7$ Å^2/ns which is about the level we observe. Shell fluctuations for droplets of this size should be best visible around $Q=0.19$ Å where within the errors we do not see maximum in D_{eff}. This might be due to the fact that the core is reduced to the AOT-head groups and about two water molecules per AOT why the amplitude of the fluctuations is supposed to be very small. D_{eff} at 250 K is therefore mainly given by the Q independent D_{tr}. The findings for the translational diffusion of the droplets (NSE) confirm the structural results (SANS) in the investigated temperature range.

Bending elasticity κ. The nature of the fluctuations are contained in the dimensionless mean squared amplitude $\langle |u_2|^2 \rangle$ and the decay rate λ_2. The variation in these two parameters with temperature is shown in Figs. 10(b) and 10(d). The bending elasticity κ can now be estimated from the polydispersity p measured by SANS, the radius R measured by SANS, and the λ_2 measured by NSE [52,53],

$$\kappa = \frac{1}{48}\left(\frac{k_B T}{\pi p^2} + \lambda_2 R^3 \frac{23\eta_w + 32\eta_t}{3}\right). \tag{16}$$

Figure 11 displays the bending elasticity κ as a function of temperature. For the whole investigated temperature range we find a constant bending elasticity $\kappa=(0.31\pm0.06)k_BT$. Even though we have observed by SANS that the droplet instability for this sample composition occurred around $T_s=255$ K when approaching T_s the bending elasticity does not decrease. Thus we conclude that our experimental findings do not allow to relate the AOT membrane elasticity to the low temperature structural instability of the droplets. The absolute value of $\kappa=0.3k_BT$ compares very well with the previous studies on AOT reverse water swollen micelles in other oils than toluene [42].

V. CONCLUSIONS

The structure of the ternary microemulsion consisting of AOT, D_2O, and toluene-d8 (or heptane-d16) was investigated by means of SANS between $T=290$ and 220 K. At a constant droplet volume fraction of $\phi=0.2$ we varied the molar ratio of surfactant to water ω between 3 and 12. At room temperature this mixture forms spherical water droplets surrounded by a monolayer of AOT dispersed in the continuous oil matrix with a core radius R_c proportional to ω. We found this droplet structure to be stable down to temperatures far below the freezing point of bulk water. The smaller the ω is, the lower the phase transition temperature is. For the smallest water swollen reverse micelles with $\omega=3$ ($R_c=7$ Å) the droplets were stable down to $T=232$ K. At an ω-dependent temperature T_s we observed the shrinking of the droplets. The difference ΔT between the bulk freezing point T_f of deuterated water and the shrinking temperature T_s was inversely proportional to the micelle radius R_c. Hence it followed the same dependency as the supercooling of water confined in reverse micelles determined earlier by means of neutron BS [18]. Going to even lower temperatures we observed a constant remaining water core whose size seemed to be independent of the initial droplet water loading. A direct comparison with SANS spectra from pure AOT reverse micelles dispersed in toluene-d8 allowed us to determine the amount of remaining (probably unfreezable) water to be about 2 water molecules per AOT molecule ($\omega=2$). For two samples we monitored the droplet structure upon heating back to room temperature. We showed that the structural changes observed upon cooling are fully reversible and that a continuous water uptake takes place from the lowest temperatures on. For one composition with an initial core radius $R_c=18$ Å (AOT/D_2O/toluene-d8, $\phi=0.1$, $\omega=8$) we used NSE to investigate the shell fluctuations from room temperature down to a temperature below the point T_s where the shrinking of these droplets was observed beforehand. Confirming the SANS results we found a constant hydrodynamic radius of about 1.3 times the geometrical radius (R_c+d) for all temperatures above T_s. Below T_s the translational diffusion coefficient corresponded to the size of the shrunken droplets. Analyzing the shell fluctuations we observed a relaxation rate λ_2 which increases with temperature. Nevertheless following the model proposed by Kawabata *et al.* [46] for the determination of the AOT film bending elasticity κ we did not see a variation with temperature. Contrary to results for water swollen AOT micelles in decane where the

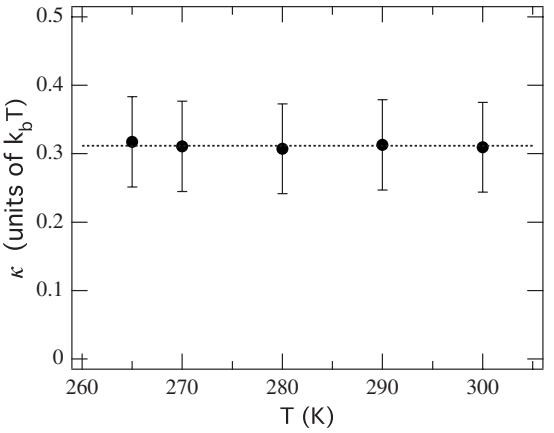

FIG. 11. Temperature dependence of bending elasticity κ of the AOT shell calculated after Eq. (16). Dotted line shows the average bending elasticity $\kappa=(0.31\pm0.06)k_BT$.

shell became more floppy (corresponding to a decreasing κ) with increasing temperature [54] our data analysis yielded a constant bending elasticity of $\kappa \approx 0.3 k_B T$ over the whole investigated temperature range where the droplets are stable. From our experimental results no relation between the droplet instability at T_s and the bending elasticity κ can be inferred. We conclude that this ternary water-in-oil droplet microemulsion can be an appropriate model system for the study of confined water over a large temperature range. It allows us to vary the size of the soft confinement: rather monodisperse droplets with water core radii ranging from a few angstroms to several nanometers can be obtained. No significant change in the AOT shell elasticity can be experimentally observed with temperature and thus the stiffness of the water enclosing membrane does not vary in a detectable way which simplifies the interpretation of water investigations. This now well characterized system has a large potential to advance the understanding of the nature of water in soft confinement with many implications also for biological systems. Inelastic neutron scattering experiments to elucidate the dynamical behavior of supercooled water in reverse micelles are in progress [43].

ACKNOWLEDGMENTS

We acknowledge the ILL for the allocated beamtime, Bela Farago (ILL) for helpful discussions and for providing us with his NSE data correction macros, and Michael Prager (Forschungszentrum Jülich) for borrowing of the sample holders.

[1] T. De and A. Maitra, Adv. Colloid Interface Sci. **59**, 95 (1995).
[2] M. Kotlarchyk, S. H. Chen, J. S. Huang, and M. W. Kim, Phys. Rev. A **29**, 2054 (1984).
[3] L. M. Wang, F. He, and R. Richert, Phys. Rev. Lett. **92**, 095701 (2004).
[4] R. Zorn, M. Mayorova, D. Richter, and B. Frick, Soft Matter **4**, 522 (2008).
[5] T. Blochowicz, E. Gouirand, A. Fricke, B. Stühn, T. Spehr, and B. Frick (unpublished).
[6] N. Levinger, Science **298**, 1722 (2002).
[7] E. Meyer, Protein Sci. **1**, 1543 (1992).
[8] P. Steinbach and B. Brooks, Proc. Natl. Acad. Sci. U.S.A. **90**, 9135 (1993).
[9] M.-C. Bellissent-Funel, Eur. Phys. J. E **12**, 83 (2003).
[10] P. Douzou, E. Keh, and C. Balny, Proc. Natl. Acad. Sci. U.S.A. **76**, 681 (1979).
[11] C. Babu, V. Hilser, and J. Wand, Nat. Struct. Mol. Biol. **11**, 352 (2004).
[12] M. Zulauf and H.-F. Eicke, J. Phys. Chem. **83**, 480 (1979).
[13] C. Boned, J. Peyrelasse, and M. Moha-Ouchane, J. Phys. Chem. **90**, 634 (1986).
[14] P. C. Schulz, J. Therm Anal. Calorim. **51**, 135 (1998).
[15] D. Senatra, Z. Zhou, and L. Pieraccini, Prog. Colloid Polym. Sci. **73**, 66 (1987).
[16] C. A. Munson, G. A. Baker, S. N. Baker, and F. V. Bright, Langmuir **20**, 1551 (2004).
[17] N. Nucci and J. Vanderkooi, J. Phys. Chem. B **109**, 18301 (2005).
[18] T. Spehr, B. Frick, I. Grillo, and B. Stühn, J. Phys.: Condens. Matter **20**, 104204 (2008).
[19] P.-O. Quist and B. Halle, J. Chem. Soc., Faraday Trans. 1 **84**, 1033 (1988).
[20] J. S. Huang, S. T. Milner, B. Farago, and D. Richter, Phys. Rev. Lett. **59**, 2600 (1987).
[21] B. Farago, D. Richter, J. S. Huang, S. A. Safran, and S. T. Milner, Phys. Rev. Lett. **65**, 3348 (1990).
[22] R. Ghosh, S. Egelhaaf, and A. Rennie, *A Computing Guide for Small-Angle Scattering Experiments*, 5th ed. (Institute Laue Langevin, Grenoble, France, 2006), Paper No. ILL06GH05T.
[23] A. Dianoux and G. Lander, *Neutron Data Booklet* (Old City Publishing, Philadelphia, PA, 2003).
[24] S. H. Chen, Annu. Rev. Phys. Chem. **37**, 351 (1986).
[25] M. Kotlarchyk, R. Stephens, and J. Huang, J. Phys. Chem. **92**, 1533 (1988).
[26] M. Kotlarchyk and S. H. Chen, J. Chem. Phys. **79**, 2461 (1983).
[27] R. J. Baxter, J. Chem. Phys. **49**, 2770 (1968).
[28] S. V. Menon, C. Manohar, and K. S. Rao, J. Chem. Phys. **95**, 9186 (1991).
[29] R. Borsali and R. Pecora, *Soft-Matter Characterization* (Springer, Berlin, 2008).
[30] S. R. Kline, J. Appl. Crystallogr. **39**, 895 (2006).
[31] F. Mezei, *Neutron Spin Echo* (Springer, Berlin, 1980).
[32] F. Mezei, C. Pappas, and T. Gutberlet, *Neutron Spin Echo Spectroscopy* (Springer, Berlin, 2002).
[33] A. Simorellis, W. Van Horn, and P. Flynn, J. Am. Chem. Soc. **128**, 5082 (2006).
[34] A. Schreiber, I. Ketelsen, and G. Findenegg, Phys. Chem. Chem. Phys. **3**, 1185 (2001).
[35] M. van Dijk, J. Joosten, Y. Levine, and D. Bedeaux, J. Phys. Chem. **93**, 2506 (1989).
[36] Y. Hendrikx, H. Kellay, and J. Meunier, Europhys. Lett. **25**, 735 (1994).
[37] M. Nagao, H. Seto, M. Shibayama, and N. Yamada, J. Appl. Crystallogr. **36**, 602 (2003).
[38] A. Longo, G. Portale, W. Bras, F. Giannici, A. Ruggirello, and V. Liveri, Langmuir **23**, 11482 (2007).
[39] T. Hellweg and D. Langevin, Phys. Rev. E **57**, 6825 (1998).
[40] T. Hellweg, A. Brulet, and T. Sottmann, Phys. Chem. Chem. Phys. **2**, 5168 (2000).
[41] B. Farago and M. Gradzielski, J. Chem. Phys. **114**, 10105 (2001).
[42] C. Kitchens, D. Bossev, and C. Roberts, J. Phys. Chem. B **110**, 20392 (2006).
[43] M. Hirai, R. Kawai-Hirai, H. Iwase, Y. Kawabata, and T. Takeda, Appl. Phys. A: Mater. Sci. Process. **74**, s1254 (2002).
[44] M. Nagao and H. Seto, Phys. Rev. E **78**, 011507 (2008).
[45] B. Farago, J. Huang, D. Richter, S. Safran, and S. Milner, Prog. Colloid Polym. Sci. **81**, 60 (1990).

[46] Y. Kawabata, M. Nagao, H. Seto, S. Komura, T. Takeda, D. Schwahn, N. L. Yamada, and H. Nobutou, Phys. Rev. Lett. **92**, 056103 (2004).
[47] S. Komura and K. Seki, Physica A **192**, 27 (1993).
[48] F. Santos, C. N. de Castro, J. Dymond, N. Dalaouti, M. Assael, and A. Nagashima, J. Phys. Chem. Ref. Data **35**, 1 (2005).
[49] D. R. Lide, *CRC Handbook of Chemistry and Physics* (CRC, Boca Raton, FL, 2004).
[50] K. Harris and L. Woolf, J. Chem. Eng. Data **49**, 1064 (2004).
[51] T. Blochowicz, C. Gögelein, T. Spehr, M. Müller, and B. Stühn, Phys. Rev. E **76**, 041505 (2007).
[52] Y. Kawabata, H. Seto, M. Nagao, and T. Takeda, J. Neutron Res. **10**, 131 (2002).
[53] K. Seki and S. Komura, Physica A **219**, 253 (1995).
[54] Y. Kawabata, H. Seto, M. Nagao, and T. Takeda, J. Chem. Phys. **127**, 044705 (2007).